Eur. Phys. J. B **3**, 477–484 (1998)

**THE EUROPEAN PHYSICAL JOURNAL B**



# A polymer chain trapped between two parallel repulsive walls: A Monte-Carlo test of scaling behavior

A. Milchev[a] and K. Binder[b]

Institut für Physik, Johannes Gutenberg-Universität Mainz 55099 Mainz, Staudinger Weg 7, Germany

Received: 21 November 1997 / Accepted: 11 December 1997

**Abstract.** An off-lattice bead-spring model of a polymer chain trapped between two parallel walls a distance $D$ apart is studied by Monte-Carlo methods, using chain lengths $N$ in the range $32 \leq N \leq 512$ and distances $D$ from 4 to 32 (in units of the maximum spring extension). The scaling behavior of the coil linear dimensions parallel to the plates and of the force on the walls is studied and discussed with the help of current theoretical predictions. Also the density profiles of the monomers across the slit are obtained and it is shown that the predicted variation with the distance $z$ from a wall, $\rho(z) \propto z^{1/\nu}$, is obtained only when one introduces an extrapolation length $\lambda$ in the description, $\rho(z) \propto [(z+\lambda)/D]^{1/\nu}$, with $\lambda \approx 0.35$. An analogous result is also obtained for Gaussian chains (where $1/\nu = 2$).

**PACS.** 61.25.Hq Macromolecular and polymer solutions; polymer melts; swelling – 07.05.Tp Computer modeling and simulation – 61.41.+e Polymers, elastomers, and plastics

## 1 Introduction

Flexible polymer chains near surfaces and in thin film geometry find longstanding theoretical attention and also have important applications [1–3]. Even the dilute case, where interactions among different chains can be neglected, and only the interactions between an isolated chain and the confining wall(s) need to be considered, has intriguing properties which are not yet fully clarified [4–10], and even less is known about semi-dilute solutions confined between walls (see *e.g.* [11,12] for a discussion); *e.g.*, one of the most basic theoretical predictions is [4] that near a planar repulsive wall the monomer density profile has a depletion zone of a width of order of the coil size, and for distances $z$ from the wall that are small compared to this width the profile increases as $z^{1/\nu}$, where $\nu$ is the exponent characterizing chain linear dimensions in good solvents ($\nu \approx 0.59$) [13]. To our knowledge, this prediction has never been clearly verified either by simulation [5] or by experiment [14] (in simulations [5] studying monomer profiles near hard walls, only rather short chain lengths $N \leq 100$ were available; the experiment [14] studying the concentration profile of polymer solutions near a solid wall dealt with a stiff polysaccharide rather than a flexible chain).

In the present paper, we address this problem again by Monte-Carlo simulation of a suitable off-lattice model [8,9,15], as well as a number of related predictions. Of particular interest is the recent relation due to Eisenriegler [10] for the force exerted by the polymer on the wall and the corresponding monomer density close to the wall, and related scaling predictions how this force changes as a function of the distance $D$ between two confining walls. We reconsider also the problem how the polymer linear dimensions change with confinement [9,16–18].

The outline of this paper is as follows: in Section 2, we briefly recall the scaling predictions and in Section 3 we describe the model and make a few comments on the simulation technique; Section 4 then presents our results on the linear dimensions of the chains and the force on the wall as functions of the two basic variables, distance $D$ between the walls and chain length $N$. Section 5 then describes our results for density profiles and pressure profiles near the walls. Section 6 then summarizes our conclusions.

## 2 Summary of scaling predictions

We consider two parallel impenetrable walls a distance $D$ apart and orient our coordinate system such that the bottom wall coincides with the $xy$-plane containing the origin, while the $z$-axis is perpendicular to both walls and the top wall then is encountered for $z = D$. For an isolated chain in between these walls under good solvent conditions, we can write scaling relations for the chain mean square gyration radius components parallel ($\|$) and perpendicular ($\perp$) to the walls [16]

$$R_{g\|}^2 = \frac{2}{3} R_{gb}^2 \tilde{R}_{\|}(D/R_{gb}), \tag{1}$$

[a] *Permanent address*: Institute of Physical Chemistry, Bulgarian Academy of Sciences, 1113 Sofia, Bulgaria.
[b] e-mail: `binder@chaplin.physik.uni-mainz.de`

$$R_{g\perp}^2 = \frac{1}{3} R_{gb}^2 \tilde{R}_\perp(D/R_{gb}), \tag{2}$$

where $R_{gb}^2$ is the mean square gyration radius in the bulk, which scales as

$$R_{gb}^2 = b^2 N^{2\nu}, \quad N \to \infty. \tag{3}$$

$b$ being some (microscopic and non-universal) length, while $\tilde{R}_\parallel$, $\tilde{R}_\perp$ are universal scaling functions. The factors 2/3, 1/3 have been arbitrarily chosen to have a simple normalization of these scaling functions in the limit $D \to \infty$ where one must recover bulk behavior and hence ($\zeta \equiv D/R_{gb}$)

$$\lim_{\zeta\to\infty} \tilde{R}_\parallel(\zeta) = \lim_{\zeta\to\infty} R_\perp(\zeta) = 1. \tag{4}$$

In contrast, in the inverse limit of narrow slits, $\zeta \ll 1$, $R_{g\perp}$ cannot exceed $D$ and thus we conclude

$$\tilde{R}_\perp(\zeta \ll 1) = c_\perp \zeta^2 \tag{5}$$

where $c_\perp$ is a universal constant, and the power $\zeta^2$ ensures that in this limit $R_{gb}$ cancels out. Most interesting, of course, is the parallel component, since there a crossover to two-dimensional behavior must occur; $R_{g\parallel}^2 \propto N^{2\nu_2}$, where the exponent $\nu_2 = 3/4$ is known exactly [19]. This behavior implies

$$\tilde{R}_\parallel(\zeta \ll 1) = c_{II} \zeta^{-2(\nu_2-\nu)/\nu} \tag{6}$$

and hence for $D \ll R_{gb}$ the parallel component of the mean square gyration radius behaves as

$$R_{g\parallel}^2 = \frac{2}{3} D^2 \left(\frac{b}{D}\right)^{2\nu_2/\nu} c_{II} N^{2\nu_2}. \tag{7}$$

$c_{II}$ in equations (6, 7) being another universal constant. It should be emphasized, however, that all these relations neglect corrections to scaling, and hence are only asymptotically valid in the limit where both $D \gg b$ and $R_{gb} \gg b$.

Next we consider the monomer density profile $\rho(z)$, which is predicted to scale as follows [4,10].

$$\rho(z) = \left(R_{gb}^{1/\nu}/D\right) \tilde{X}\left(z/R_{gb}, D/R_{gb}\right), \tag{8}$$

with $\tilde{X}$ another universal scaling function. In the limit where $R_{gb} \to \infty$ at fixed $D$ equation (8) should reduce to a limit where $R_{gb}$ has cancelled out from the arguments of the scaling function, and hence

$$\rho(z) = R_{gb}^{1/\nu} D^{-1} \tilde{X}^I(z/D), \ R_{gb} \gg D. \tag{9}$$

with $\tilde{X}^I$ being another universal scaling function, while in the opposite case $R_{gb} \ll D$ and $z \ll D$ we can conclude that the profile near the left wall should approach a limiting form characteristic for the semi-infinite system,

$$\rho(z) = R_{gb}^{1/\nu} D^{-1} \tilde{X}^{II}\left(z/R_{gb}\right), \ R_{gb} \ll D. \tag{10}$$

Note that here we have followed the convention of Eisenriegler [10] to normalize the monomer density by the *polymer* density $n_b$ (number of polymer chains per unit volume) of the bulk polymer solution in the system, such that a sensible single-chain limit can be taken. The total density resulting from equation (10) is of the order $R_{gb}^{1/\nu} n_b \propto N n_b$ which is a sensible normalization of the monomer density in the dilute solution, of course.

Considering now the limit $z/R_{gb} \ll 1$ in equations (8, 10) it has been argued [4,10] that a simple power law $\rho(z) \propto z^{1/\nu}$ results,

$$\rho(z) = \frac{1}{D} z^{1/\nu} \tilde{X}^{III}(D/R_{gb}) \to \frac{1}{D} z^{1/\nu} c_\rho \text{ for } D \to \infty, \tag{11}$$

with $\tilde{X}^{III}$ being another universal scaling function, and $c_\rho$ another universal constant, respectively. Of course, it is understood that $z$ should still be large in comparison with microscopic lengths, and this makes the observability of this regime difficult.

A qualitative explanation of equation (11) is that for $z = R_{gb}$ there should be a smooth crossover from the power law to the average density due to the polymer chain confined between the walls, which is simply $N/D$ (for our single chain problem, density is not normalized per volume but per volume divided by the area of the walls, to obtain a sensible limit). Using now equation (3) we find from equation (11) from this argument $\rho(z = R_{gb}) \approx \frac{1}{D} b^{1/\nu} N c_\rho \propto N/D$, as required.

The last quantity that we discuss is the mean repulsive force $f$ exerted on the wall. For a single chain this is defined taking the derivative of the logarithm of the chain partition function with respect to the position of the wall (in the $-z$ direction). In the case of a semi-infinite system exposed to a dilute solution of polymer chains at polymer density $n_b$, one can equate the pressure on the wall to the pressure in the bulk which is simply given by the ideal gas law ($n_b k_B T$). The conclusion then is that [10]

$$\rho(z)/z^{1/\nu} = B f/k_B T, \ z \ll R_{gb}, \ z \ll D \tag{12}$$

where $B$ is an universal constant which is very close to two. Combining equations (11, 12) we can also write

$$f/k_B T = \frac{1}{D} B^{-1} \tilde{X}^{III}(D/R_{gb}). \tag{13}$$

In the wide slit limit, $D \gg R_{gb}$, $\tilde{X}^{III}$ tends to the constant $c_\rho$ and thus $f/k_B T \propto 1/D$. In the narrow slit limit, one expects that the force becomes ultimately proportional to the chain length $N$ and hence $\tilde{X}^{III}$ for $D \ll R_{gb}$ must behave as [10]

$$\tilde{X}^{III}(D/R_{gb}) \propto (D/R_{gb})^{-1/\nu}. \tag{14}$$

## 3 The model and the simulation technique

For the sake of simulation efficiency, we use a coarse-grained bead-spring model [8,9,12,15] where each effective bond is described by the Finitely Extensible Nonlinear Elastic (FENE) potential, where the bond length $l$

can vary between $l_{min} = 2l_0 - l_{max}$ and $l_{max}$, $l_0$ being the preferred distance,

$$U_{FENE}(l) = -\frac{1}{2}K(l_{max} - l_0)^2 \times \ln\left\{1 - (l - l_0)^2/(l_{max} - l_0)^2\right\}. \quad (15)$$

We choose $l_{max} = 1$ as our unit of length, $l_0 = 0.7$, so that $l_{min} = 0.4$, and the reduced spring constant $K/k_BT = 40$, *i.e.* rather large so mostly $l$ does not differ much from $l_0$, and the potential is nearly harmonic ($U \approx K(l - l_0)^2/2$).

The chains are treated as fully flexible, neither bond-angle potentials nor torsional potentials occur. The non-bonded interaction between the beads is represented by a Morse potential,

$$U_M(r)/\varepsilon_M = \exp\left[-2\alpha(r - r_{min})\right] - 2\exp\left[-\alpha(r - r_{min})\right]. \quad (16)$$

with parameters $\varepsilon_M/k_BT = 1.0$, $\alpha = 24$, $r_{min} = 0.8$. This potential may look rather special, but it turns out that it is particularly computationally convenient: the decay of this potential with distance is so rapid [15], that $U_M(r) \approx 0$ for $r > 1$ with negligible error; this allows the use of a link-cell algorithm with a cell linear dimension of unity and leads to a reasonably fast performance of our Monte-Carlo program. Using the more common truncated and shifted Lennard-Jones interaction [17,20] would deteriorate the program performance. Since the Theta temperature [13] where a single coil in dilute solutions in the bulk behaves as an ideal random walk occurs for $T = 0.62$ in the present model [15], choosing units $\varepsilon_M = 1$, $k_B = 1$, our choice of temperature $T = 1$ implies that we work in the good solvent regime, basically equation (16) acts as an excluded volume interaction with a range slightly smaller than $r_{min}$. These choices of parameters also ensure that the approach to the scaling regime, where simple power laws such as equation (3) hold, is rather rapid for the present model. The fact that the present model is well tested and its properties in the bulk have been extensively studied [15], also at semidilute concentrations and in the melt, is a further argument in favor of the choice of this model. In particular, preliminary results for some properties for small values of slit thickness $D$ and short chains have been reported already [9].

Monte-Carlo sampling of configurations is done by selecting a bead at random for an attempted move, which consists of choosing displacements $\Delta x$, $\Delta y$, $\Delta z$ drawn uniformly from the intervals $-0.5 \le \Delta x, \Delta y, \Delta z \le +0.5$. From this trial position $\mathbf{r}^I = \mathbf{r} + \Delta\mathbf{r}$ (where $\Delta\mathbf{r} = (\Delta x, \Delta y, \Delta z)$) of the monomer and the specified potentials equations (15, 16), the transition probability $W$ is computed as usual [21] from the energy change $\Delta U$ caused by this trial move,

$$W = min\left[1, \exp\left(-\Delta U/k_BT\right)\right]. \quad (17)$$

The attempted move is accepted only if $W$ exceeds a random number $\eta$, uniformly distributed in the interval $0 \le \eta < 1$. The performance of this algorithm is about

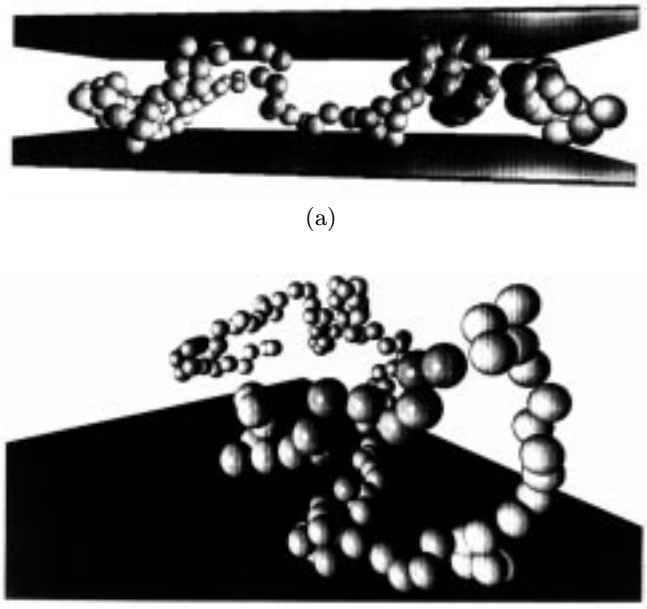

(a)

(b)

**Fig. 1.** Snapshot pictures of chains of length $N = 128$ confined between two repulsive walls at a distance $D = 4$ (a) and $D = 16$ (b). Each bead is represented by a sphere of diameter 0.8, while the springs between the beads are not shown.

$5 \times 10^4$ attempted updates per monomeric units per CPU second on workstations such as IBM RS 6000/370. We choose system linear dimensions $L \times L \times D$, with $D = 4$, 8, 16, 32 (unlike previous work [9,17] where $D$ was much smaller and thicknesses of order $D = 1$ were included, *i.e.* slit thicknesses of the order of the bond length, for which case it is doubtful that one should expect the scaling behavior as described in Sect. 2). In the $x$ and $y$ directions parallel to the walls, periodic boundary conditions were used. Chain lengths used were $N = 32$, 64, 128, 256 and 512, and the lateral linear dimension typically was $L = 64$ (only for $N = 512$ and $D = 8$, 16 , 32 a smaller size, $L = 32$, was used for technical reasons). Typical acceptance rate for the moves described above is about 13%, while for the case of Gaussian chains with the interaction in equation (16) turned off the acceptance rate increased up to 30% (such chains without excluded volume interaction were studied for comparison in some cases). Typical length of individual runs was $10^7$ Monte-Carlo Steps (MCS) per monomer, and 20 independent runs were made for each combination of parameters $(N, D)$, allowing a reliable estimation of statistical errors. Figure 1 gives a pictorial impression of the chain configurations generated.

Finally we remark that the pressure tensor is obtained from the virial theorem [12,22]

$$\rho_{\alpha\beta}(z) = \rho(z)k_BT\delta_{\alpha\beta} - (6V)^{-1}\sum_{i\neq j}(\mathbf{r}_{ij})_\alpha \frac{\partial U(\mathbf{r}_{ij})}{\partial(\mathbf{r}_{ij})\beta}\left[\delta(z_i - z) + \delta(z_j - z)\right] \quad (18)$$

**Table 1.** Linear dimensions of the chain and force on the walls.

| $D$ | $N$ | $R^2_{g\|\|}$ | $R^2_{g\perp}$ | $R^2_{\|\|}$ | $R^2_{\perp}$ | $f$ |
|---|---|---|---|---|---|---|
| | 128 | 38.54 | 0.739 | 274.0 | 2.126 | 1.76 |
| 4 | 256 | 124.8 | 0.751 | 943.9 | 2.122 | 3.38 |
| | 512 | 291.7 | 0.763 | 1802 | 2.125 | 7.35 |
| | 128 | 30.06 | 2.391 | 199.7 | 7.839 | 0.421 |
| 8 | 256 | 70.67 | 2.597 | 509.5 | 7.841 | 0.733 |
| | 512 | 217.1 | 2.735 | 1627 | 8.029 | 1.484 |
| | 512 (g) | 129.6 | 2.451 | 917.7 | 7.503 | |
| | 128 | 25.51 | 6.373 | 165.7 | 28.7 | 0.111 |
| 16 | 256 | 62.14 | 8.398 | 422.0 | 29.54 | 0.179 |
| | 512 | 140.8 | 9.423 | 797.2 | 29.91 | 0.917 |
| | 512 (g) | 94.70 | 8.325 | 671.7 | 30.38 | |
| | 128 | 23.74 | 10.09 | 151.6 | 59.84 | 0.0403 |
| 32 | 256 | 55.07 | 18.65 | 349.0 | 99.11 | 0.0573 |
| | 512 | 120.1 | 29.12 | 719.6 | 114.8 | 0.0868 |
| | 512 (g) | 75.36 | 18.75 | 499.5 | 87.13 | |

where $U(\mathbf{r}_{ij})$ is the sum of all potentials, equations (15, 16). The pressure on the walls equals the average pressure in the film in thermal equilibrium. The force due to the polymer is then obtained multiplying by the area $L^2$ of the system.

## 4 Linear dimensions of the chains and force on the wall: test of scaling behavior

In Table 1 we summarize the numerical results found in the present work for the parallel and perpendicular parts of the mean square gyration radius, $R^2_{g\|}$ and $R^2_{g\perp}$, as well as the corresponding components of the end to end distance, $R^2_{\|}$ and $R^2_{\perp}$, and finally we show the force on the walls, $f$ (remember our choice of units, $k_B \equiv 1$, and temperature $T = 1$). Only chain lengths $N > 128$ are included here, and in a few cases results for Gaussian chains [labelled as 512(g)] are included for comparison. Note, however, that the statistical errors of the present calculations are still rather large for the parallel components, the error there may already affect the second digit shown, while for the perpendicular components and the pressure it only affects the third digit.

The rather large errors (particularly for the parallel components) introduce also some scatter in the scaling plots, Figures 2, 3 and 4. Thus the deviations from scaling in Figure 2 are presumably simply due to these statistical errors, while in the force data some systematic effects are clearly visible, although the general trends of the scaling functions do follow the theoretical predictions sketched in Section 2, as shown by the straight lines showing the asymptotic slopes of the scaling functions. We have no clear explanation why in the force data there are still rather pronounced corrections to scaling present. At this point, we mention that Webman *et al.* [17] have studied the scaling of the radii (analoguous to our Figs. 2, 3) for much shorter chains ($20 \leq N \leq 80$) and thinner slits ($0.68 \leq D/a \leq 6.74$, where a is the bond length of that model) and found rather good agreement with the scaling description. It would be interesting to study also the pressure on the walls, using the model of [17].

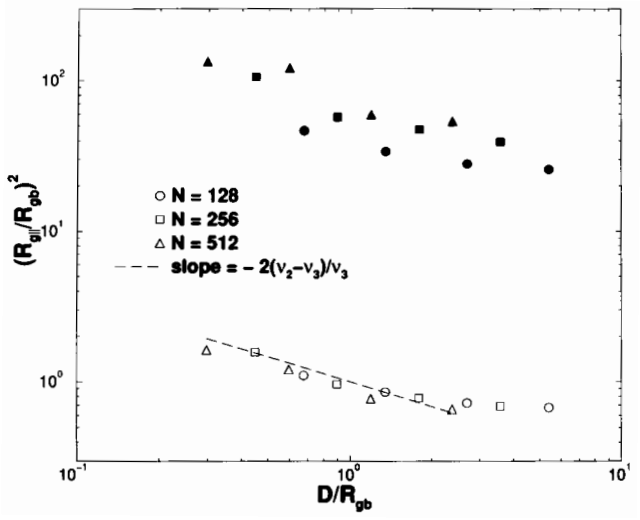


**Fig. 2.** Plot of the normalized parallel component of the mean square gyration radius, $R^2_{g\|}/R^2_{gb}$, open symbols, and end-to-end distance, $R^2_{\|}/R^2_{gb}$ full symbols, *versus* the ratio $D/R_{gb}$ (chain lengths $N = 128$, 256 and 512 are distinguished by different symbols. Dashed straight line indicates the asymptotic slope of the scaling function for small $D/R_{gb}$, namely $-2(\nu_2 - \nu)/\nu$.

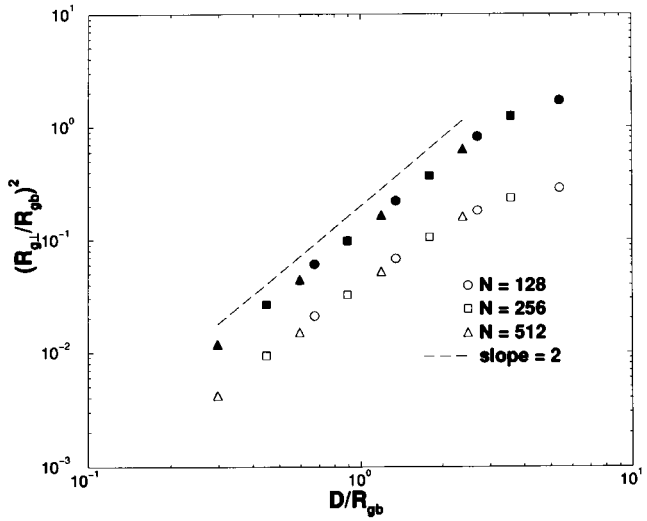


**Fig. 3.** Same as Figure 2, but for the perpendicular components. Dashed line indicates the asymptotic slope for small $D/R_{gb}$, namely 2.

## 5 Density profiles for single chains in a slit

Figures 5 to 9 show the main results of the present investigation, namely the density profiles, plotted in log-log

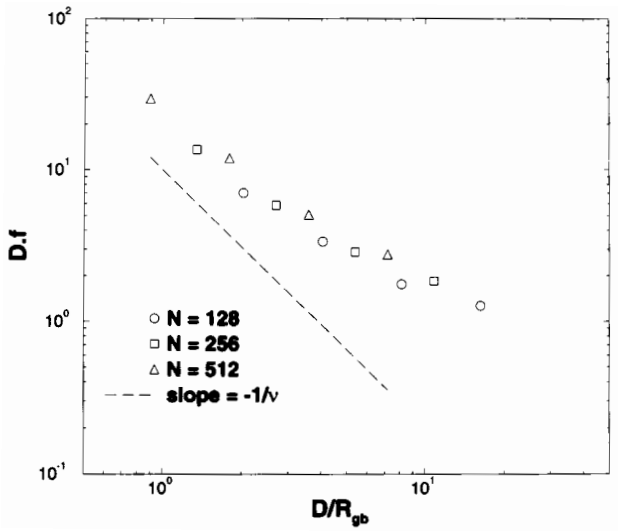


**Fig. 4.** Scaling plot for the force, $Df$ *versus* $D/R_{gb}$. The dashed straight line indicates the slope that the scaling function should exhibit for small $D/R_{gb}$.

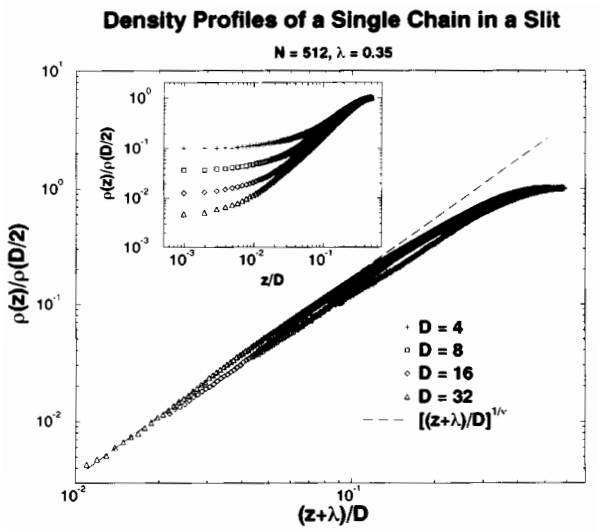


**Fig. 5.** Density profiles $\rho(z)$, normalized by the density $\rho(D/2)$ in the center of the slit, on a log-log plot *versus* the modified relative distance from the left wall, $(z+\lambda)/D$. Here the extrapolation length $\lambda = 0.35$. Four thicknesses of the slit are included, as indicated. Dashed line gives the predicted power-law behaviour, $[(z+\lambda)/D]^{1/\nu}$. Inset shows the same data but plotted *versus* $z/D$, *i.e.* without taking an extrapolation length into account. Chain length is $N = 512$.

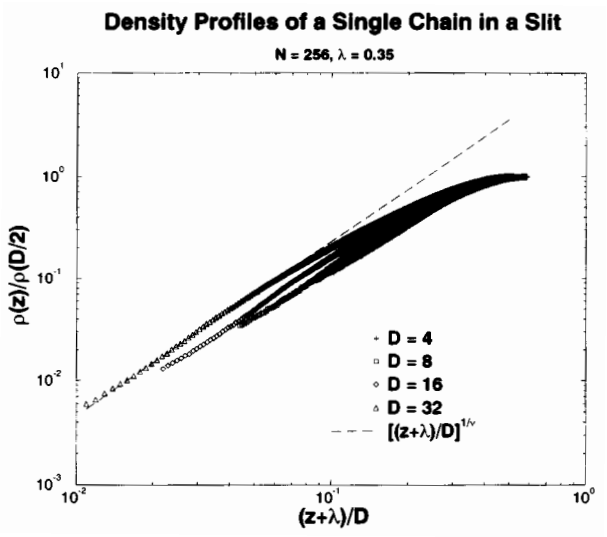


**Fig. 6.** Same as Figure 5 but for $N = 256$.

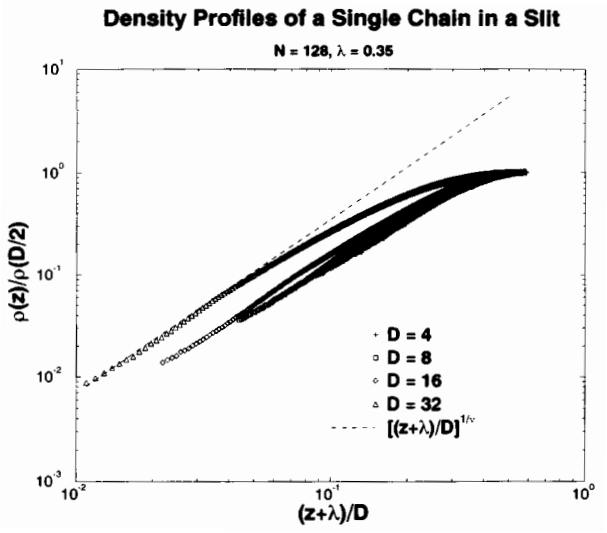


**Fig. 7.** Same as Figure 5 but for $N = 128$.

form to check for the power law, equation (11). As it is seen from the "raw data" presented in the insert to Figure 5, the data for $z/D \ll 1$ settle down to constant values, and a region where $z/D$ is still small and a power law is seen cannot be easily identified. This observation does not mean, however, that the theory outlined in equations (8−11) of Section 2 is wrong – this scaling theory is expected to hold only for distances $z$ "large on the microscopic scale" [10]. Studying such a regime where $z$ is very large in comparison to microscopic scales, but very small in comparison with $D$ as well as $R_{gb}$, is very hard with simulations, it does require to choose both $N$ and $D$ extremely large.

Fortunately, to leading order the effects of the microscopic scale can be incorporated in the treatment by using the concept of the "extrapolation length" [23–25], well known from the theory of surface effects on magnetic phase transitions (which are equivalent to the case of polymers at surfaces [2,5,10] in the framework of the mapping [13] to the $n$-vector model of magnetism in the limit $n \to 0$). This means that in equations (11, 12) the power $z^{1/\nu}$ should be replaced by $(z+\lambda)^{1/\nu}$. For $z \gg \lambda$, of course, this correction does not alter the description of the scaling behavior. But as Figure 5 shows, fitting $\lambda$ such that the bending to horizontal plateaus seen in the insert just disappears gives a straightforward fit to the law $\rho(z) \propto (z+\lambda)^{1/\nu}$ over a wide parameter range.

The value obtained for $\lambda$, $\lambda = 0.35$, has an obvious physical interpretation in our model since this is just one

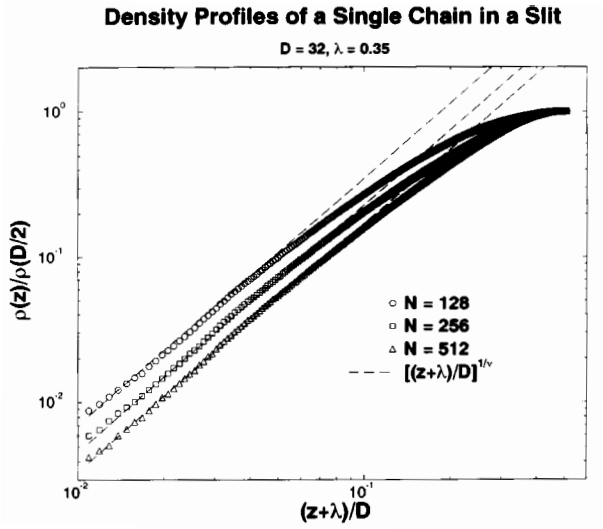


**Fig. 8.** Log-log plot of normalized density profiles *vs.* $(z+\lambda)/D$ for $D = 32$, for three chain lengths as indicated. Broken straight line indicate the behavior $[(z+\lambda)/D]^{1/\nu}$.

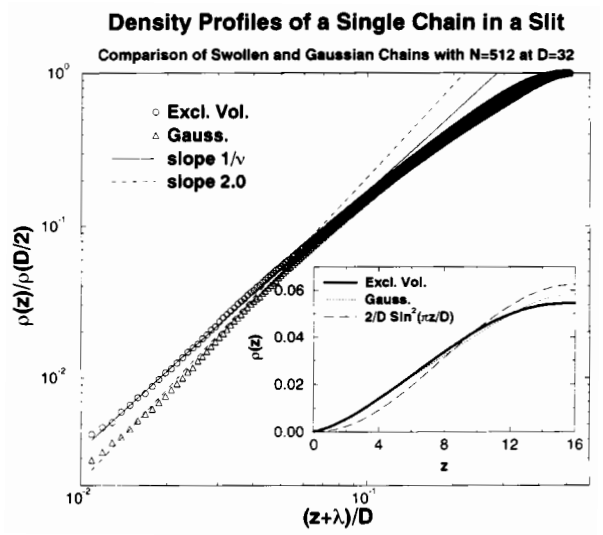


**Fig. 9.** Log-log plot of the density profiles $\rho(z)$, normalized by $\rho(D/2)$, plotted *vs.* $(z+\lambda)/D$ for the case $N = 512$, $D = 32$, and comparing chains with excluded volume interactions (Eq. (16)), circles, and chains without them, triangles. The extrapolation length $\lambda = 0.35$ was used for both cases. Straight lines show the predicted slopes. Insert shows $\rho(z)$ *vs.* $z$, including also the corresponding analytical result $(2/D)\sin^2(\pi z/D)$ for Gaussian chains with the boundary condition $\rho(z=0) = 0$.

half of the preferred bond length, $l_0 = 0.7$, *cf.* equation (15). Of course, for this concept of an extrapolation length to make sense, it is of crucial importance to show that $\lambda$ indeed is a microscopic length, *i.e.* it cannot depend on mesoscopic parameters like the slit width $D$ and the gyration radius $R_{gb}$ (or the chain length $N$, respectively) of the polymers. Figures 5–8 demonstrate that this requirement indeed is very well fullfilled, and for large $D$

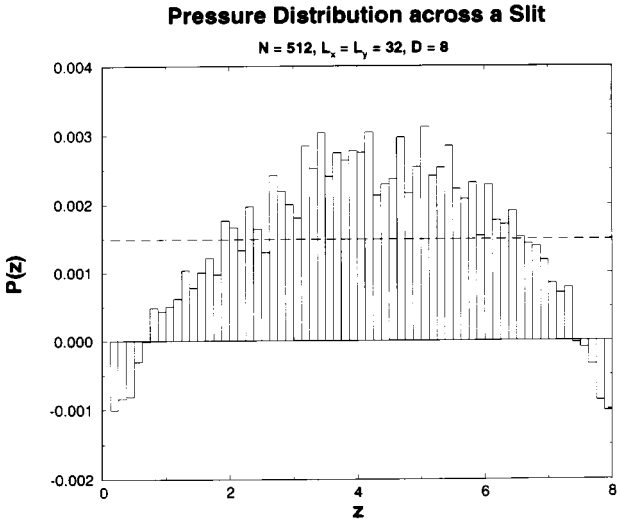


**Fig. 10.** Distribution of the local pressure $P(z) \equiv \sum_\alpha p_{\alpha\alpha}(z)$ as a function of the distance $z$ from the left wall across the slit, for the case $N = 512$, $L = 32$, $D = 8$. The horizontal dashed line indicates the resulting average pressure, need to obtain the force $f$ in Figure 4 ($f = PL^2$).

and large $N$ the correct slope $1/\nu$ can be seen over a full decade in $(z+\lambda)/D$.

To test this concept of the extrapolation length further, we also simulated Gaussian chains by turning off the Morse potential, equation (16), but keeping the FENE-potential equation (15) between the beads. Figure 9 shows that also in this case the same choice of $\lambda = 0.35$ is needed in order to verify $\rho(z) \propto (z+\lambda)^{1/\nu_{MF}} = (z+\lambda)^2$ over a wide range (remember $\nu_{MF} = 1/2$). The asymptotic result for Gaussian chains in a narrow slit, where $\lambda$ is neglected, namely [10] (note that in Fig. 9 the integral of the density was normalized to one rather than to $N$)

$$\rho(z) = \frac{2}{D}\sin^2(\pi z/D) \tag{19}$$

deviates from the observed density profile markedly, even for Gaussian chains as long as $N = 512$ beads! This observation shows again that for many phenomena of interest it is not only important to consider some asymptotic scaling law, but it is important to understand how effects on short length scales change the picture. We feel that Figures 5–9 demonstrate clearly that the use of a suitable extrapolation length is an adequate procedure for monomer density profiles of dilute polymer solutions near hard walls.

Our calculations not only yield density profiles but also pressure profiles, though with less accuracy (Fig. 10). These data were used to obtain the average pressure in the slit and hence the normal force on the wall. It should be noted that in regions with a strong density variation the local pressure $P(z)$ can become negative (this happens also for the local pressure in a gas-liquid interface according to the van der Waals-Cahn-Hilliard type description of such an interface [26]), and hence it is not too surprising that here this happens close to the wall. In the wide slit limit $D/R_{gb} \gg 1$, we would expect that the density $\rho(z)$

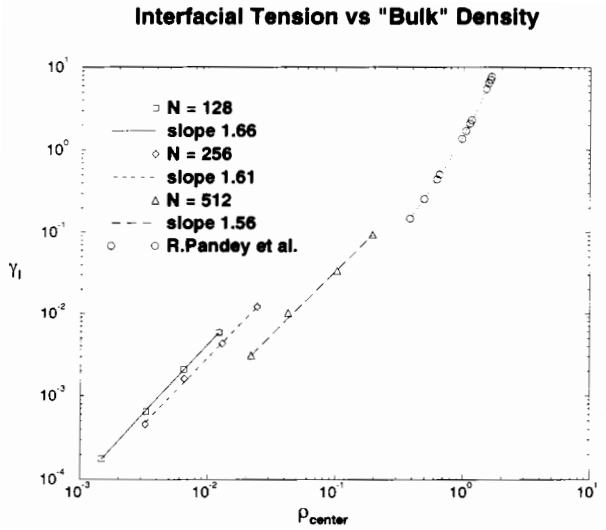


**Fig. 11.** Log-log plot of the effective interface tension $\gamma_I$ plotted *vs.* the density $\rho_{center}$ in the center of the slit (from the density $\rho(z)$ normalized as $\int_O^D \rho(z)dz = 1$ as shown in Fig. 9 $\rho_{center}$ is obtained as $\rho_{center} = \rho(z = D/2)N/L^2$). Data for semidilute solutions for $N = 32$ from Pandey *et al.* [12] are included.

for $z > R_{gb}$ but $z < D - R_{gb}$ is essentially constant, representing a dilute polymer solution at a density close to $N/(DL^2)$ in the slit. For this limit, it is of interest to obtain the surface free energy associated with the repulsive wall from [12,27]

$$\gamma_I = \frac{1}{2}\int_O^D dz\big[p_{zz}(z) - \big(p_{xx}(z) + p_{yy}(z)\big)/2\big]. \qquad (20)$$

Figure 11 shows a log-log plot of the data obtained for $\gamma_I$ from equation (20) as function of the density in the center of the film. Data from Pandey *et al.* [12] for a multi-chain system with $N = 32$ are included. While in the latter simulation actually a homogeneous situation in the center of the film was established, where $p_{zz}(z) = p_{xx}(z) = p_{yy}(z)$ independent of $z$ for some region in the center of the slit, this is not the case here (the data of Fig. 11 refer in part to the narrow slit limit $D/R_{gb} \lesssim 1$ rather than the wide slit limit $D/R_{gb} \gg 1$, and therefore $p_{zz}(z) \neq p_{xx}(z) = p_{yy}(z)$ even in the center of the slit). It is seen that the data for $\gamma_I$ obtained in this way scale as $\gamma_I \propto \rho_{center}^{\kappa}$ with an exponent $\kappa$ approximately equal to $1/\nu \approx 1.695$.

Finally we return to the question of the universal constant $B$ defined in equation (12). Since we have seen that it is appropriate to introduce the extrapolation length $\lambda$ as a correction in the density profile, we define ($R_x \equiv \sqrt{\langle R^2\rangle/3}$, $\langle R^2\rangle$ being the mean square end to end distance in the bulk) [10].

$$B_{eff} = \left(R_x^{1/\nu}/N\right)\rho(z)/\left[(z+\lambda)^{1/\nu} f/k_BT\right]. \qquad (21)$$

Normalizing the densities such that $\int_O^D \rho(z)dz = N$, we hence obtain for $D = 32$ that $B_{eff}(N = 128) \approx 2.48$, $B_{eff}(N = 256) \approx 2.53$, and $B_{eff}(N = 512) \approx 2.68$, while for $D = 16$ we get $B_{eff}(N = 128) \approx 2.85$, $B_{eff}(N = 256) \approx 3.44$, $B_{eff}(N = 512) \approx 3.46$, and still larger values result for $D = 8$, $B_{eff}(N = 128) \approx 3.67$, $B_{eff}(N = 256) \approx 4.19$, $B_{eff}(N = 512) \approx 4.12$. Thus all these estimates for $B_{eff}$ have the same order of magnitude, but they are not universal. There is a systematic decrease of $B_{eff}$ with increasing $D$. Presumably the correct value for the universal number $B$ is only obtained if one considers the limit $D \to \infty$ and still longer chains. In view of these problems, it is of course premature to compare $B_{eff}$ to the estimate of Eisenriegler (which is $B \approx 1.85$, in first order expansion in $\varepsilon = 4-d$) [10]. Plotting $B_{eff}$ *versus* $1/\sqrt{D}$ a rather rough linear extrapolation is possible which would yield an extrapolated result $B \approx 1.4$. Clearly, more simulation work is possible to resolve this problem, and also an $\varepsilon$-expansion result to higher order would be very desirable.

## 6 Conclusions

In this paper, the depletion of the density profile of very dilute polymer solutions near hard walls has been studied by Monte-Carlo simulations of a (coarse-grained) bead-spring model of polymer chain confined in a slit. It was shown that the density profile can be described by a power law, $\rho(z) \propto (z+\lambda)^{1/\nu}$, where the extrapolation length $\lambda$ is independent of both chain length $N$ and slit width $D$, but is a nonuniversal length that depends on the characteristics of our model (and the details of the wall-monomer interaction, of course, which in our case was purely repulsive). Even for our longest chains ($N = 512$ beads), a limit $\lambda \ll z \ll R_{gb}$ cannot be reached, and no power law could be identified without taking the extrapolation length into account. Since each effective bond of our chain is comparable to the persistence length of a real chain, comprising several chemical monomers, it is clear that also in real systems containing polymers with a degree of polymerization of the order $10^3$ to $10^4$ the analogous correction due to an extrapolation length will not be negligible either.

We have also studied the scaling behavior of the parallel and perpendicular chain linear dimensions of the chain confined by the slit, as well as for the force $f$ exerted on the walls. Within some scatter – part of it is statistical but part is systematic due to corrections to scaling – the proposed scaling relations are satisfied (Figs. 2–4). Unfortunately, we have not been able to study the wide slit limit where $Df$ is independent of $D$, and thus meaningful estimates for the universal amplitude $B$ defined by Eisenriegler [10] could not yet be obtained.

This research was supported by the Deutsche Forschungsgemeinschaft (DFG) under grant N° 436BUL113/92 and by the Bulgarian National Science Foundation under grant X-301. We are grateful to Prof. E. Eisenriegler for stimulating discussions and helpful comments comments on the manuscript.

## References


1. P.-G. de Gennes, Adv. Colloid Interf. Sci. **27**, 189 (1987).
2. E. Eisenriegler, *Polymers Near Surfaces* (World Scientific, Singapore 1993).
3. G.J. Fleer, M.A. Cohen-Stuart, J.M.H.J. Scheutjens, T. Cosgrove, B. Vincent, *Polymers at Interfaces* (Chapman & Hall, London 1993).
4. J.F. Joanny, L. Leibler, P.-G. de Gennes, J. Polym. Sci, Polym. Phys. Ed. **17**, 1073 (1979).
5. E. Eisenriegler, K. Kremer, K. Binder, J. Chem. Phys. **77**, 6296 (1982).
6. S. Livne, H. Meirovitch, J. Chem. Phys. **88**, 4498 (1988); H. Meirovitch, S. Livne, J. Chem. Phys. **88**, 4507 (1988).
7. P.-Y. Lai, J. Chem. Phys. **103**, 5742 (1995); Macromol. Theory Simul. **5**, 255 (1996).
8. A. Milchev, K. Binder, Macromol. **29**, 343 (1996).
9. A. Milchev, K. Binder, J. Phys. II. France **6**, 21 (1996).
10. E. Eisenriegler, Phys. Rev. E **55**, 3116 (1997).
11. K. Binder, A. Milchev, J. Baschnagel, Annu. Rev. Mater. Sci. **26**, 107 (1996).
12. R.B. Pandey, A. Milchev, K. Binder, Macromol. **30**, 1194 (1997).
13. P.-G. de Gennes, *Scaling Concepts in Polymer Physics* (Cornell University Press, Ithaca 1979).
14. D. Ausseré, H. Hervet, F. Rondelez, Phys. Rev. Lett. **54**, 1948 (1985).
15. A. Milchev, W. Paul, K. Binder, J. Chem. Phys. **99**, 4786 (1993); I. Gerroff, A. Milchev, K. Binder, W. Paul, J. Chem. Phys. **98**, 6526 (1993); A. Milchev, W. Paul, K. Binder, Macromol. Theory Simul. **3**, 305 (1994); A. Milchev, K. Binder, Macromol. Theory Simul. **3**, 915 (1994).
16. M. Daoud, P.-G. de Gennes, J. Phys. France **38**, 85 (1977).
17. I. Webman, J.L. Lebowitz, M.H. Kalos, J. Phys. France **41**, 579 (1980).
18. K. Kremer, K. Binder, J. Chem. Phys. **81**, 638 (1984).
19. B. Nienhuis, J. Stat. Phys. **34**, 731 (1984).
20. K. Kremer, G.S. Grest, J. Chem. Phys. **92**, 5097 (1990).
21. *Monte-Carlo and Molecular Dynamics Simulations in Polymer Science*, edited by K. Binder (Oxford University Press, New York 1995).
22. M.P. Allen, D.J. Tildesley, *Computer Simulation of Liquids* (Clarendon, Oxford 1987).
23. K. Binder, *Phase Transitions and Critical Phenomena*, edited by C. Domb, J.L. Lebowitz, Vol. 8.
24. K. Binder, P.C. Hohenberg, Phys. Rev. B **6**, 3461 (1972).
25. D.P. Landau, K. Binder, Phys. Rev. B **41**, 4633 (1980).
26. B. Widom, J. Rowlinson, *Molecular Theory of Capillarity* (1982).
27. B. Smit, Phys. Rev. A **37**, 3481 (1988).